



Supplementary Material for

Transition from turbulent to coherent flows in confined three-dimensional active fluids

Kun-Ta Wu, Jean Bernard Hishamunda, Daniel T. N. Chen, Stephen J. DeCamp, Ya-Wen Chang, Alberto Fernández-Nieves, Seth Fraden,* Zvonimir Dogic*

*Corresponding author. Email: fraden@brandeis.edu (S.F.); zdogic@brandeis.edu (Z.D.)

Published 24 March 2017, *Science* **355**, eaal1979 (2017)
DOI: 10.1126/science.aal1979

This PDF file includes:

Figs. S1 to S6

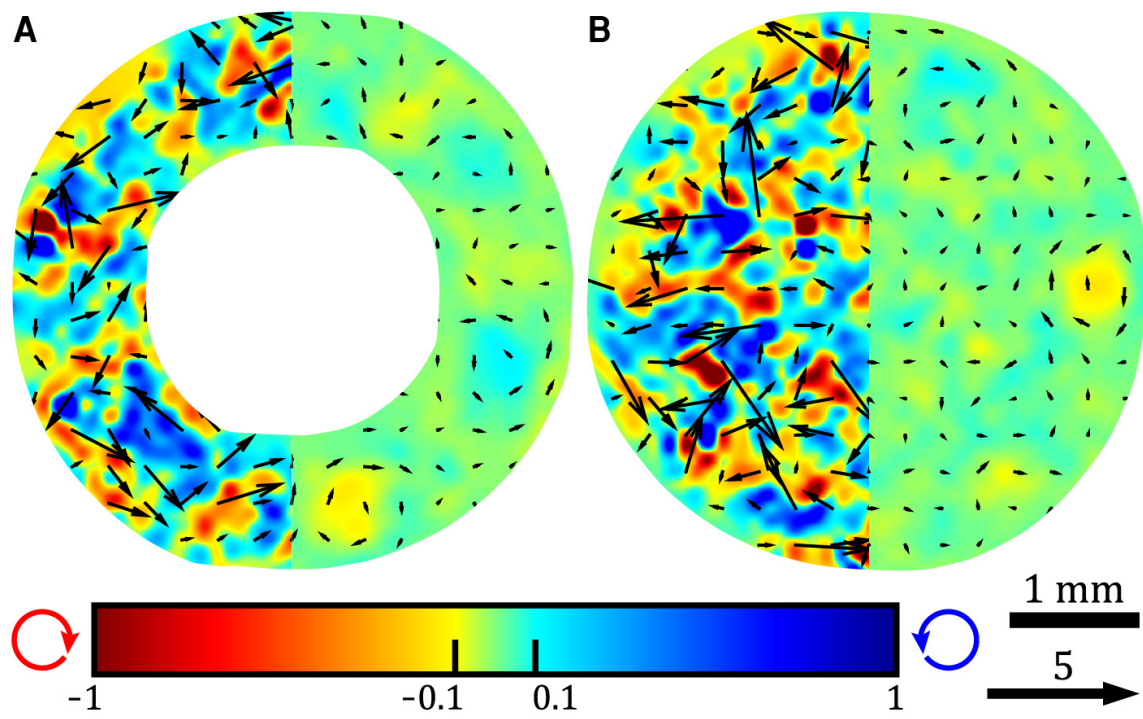


Fig. S1. Geometrical confinements with large aspect ratios suppress coherent flows. (A) Incoherent flow in a toroidal geometry, with low circulation order parameter ($\Phi = 0.02$). Coherent flows were suppressed by reducing the height of the confining geometry from 1.3 to 0.33 mm (Fig. 1E). (B) Incoherent flow in cylinder with low circulation order parameter ($\Phi = 0.03$). To suppress coherent flows the height was reduced from 1.3 to 0.33 mm (Fig. 1F).

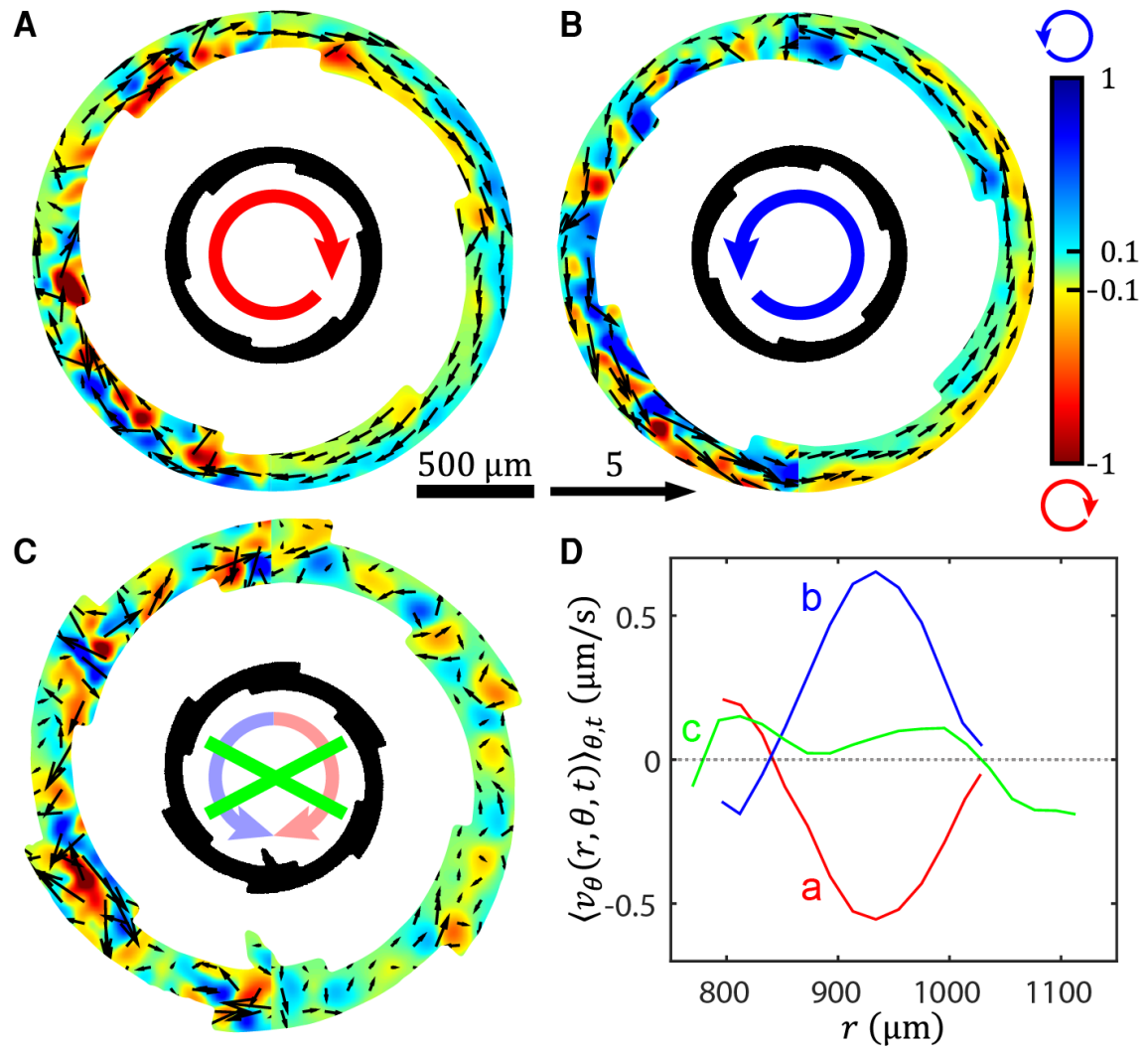


Fig. S2

Ratchet geometries that suppress coherent flows. (A) Clockwise circular flow directed by counter-clockwise saw-teeth decorating the inner toroid surface. Channel height is 70 μm . (B) Clockwise notches on the inner toroid surface direct counter-clockwise circulation. (C) Inner and outer saw-teeth patterns of the same handedness induce flows with the opposite handedness (Fig. 3A), consequently suppressing coherent flows. (D) Velocity profiles of the self-organized flows in geometries shown in panels A-C.

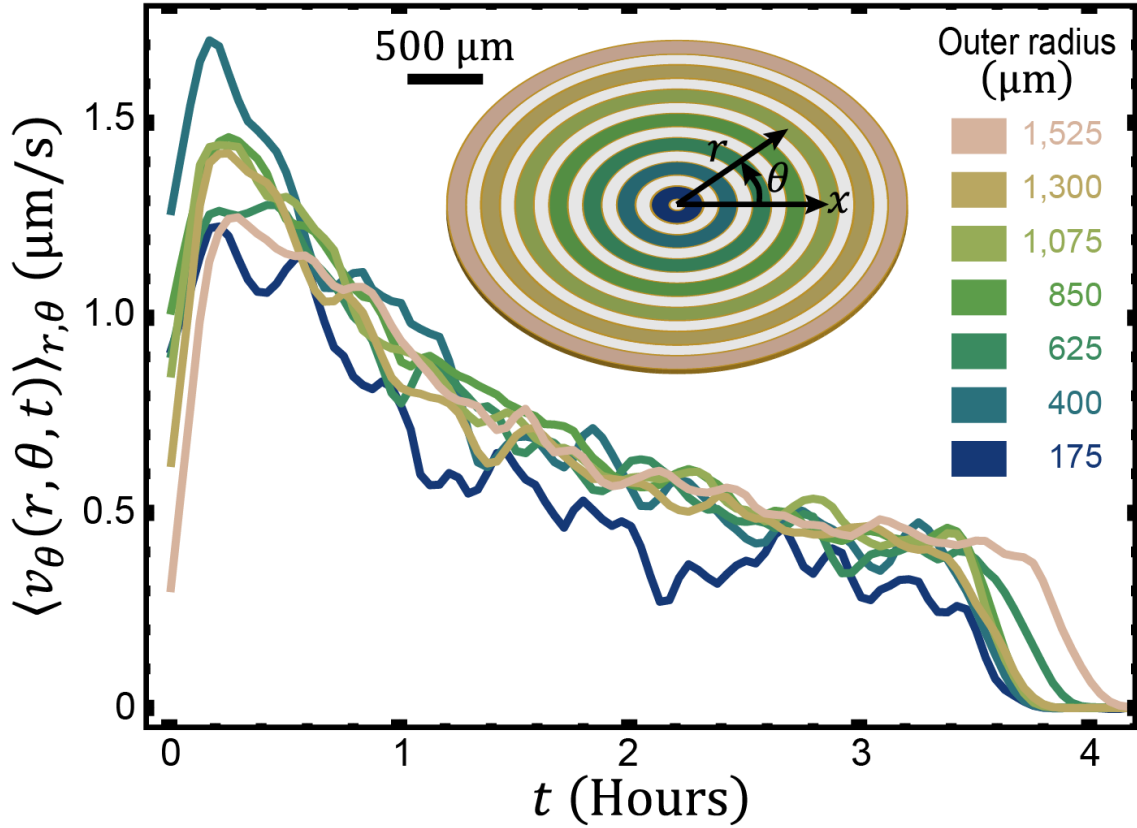


Fig. S3 Flow profiles are independent of the toroid radius and curvature. Evolution of the mean azimuthal velocities plotted for seven concentric toroids whose radii range from 175 to 1,525 μm . Flow velocities in toroids with different radii evolve similarly, demonstrating that the coherent flows are independent of the confinement curvature. Toroid heights are 60 μm .

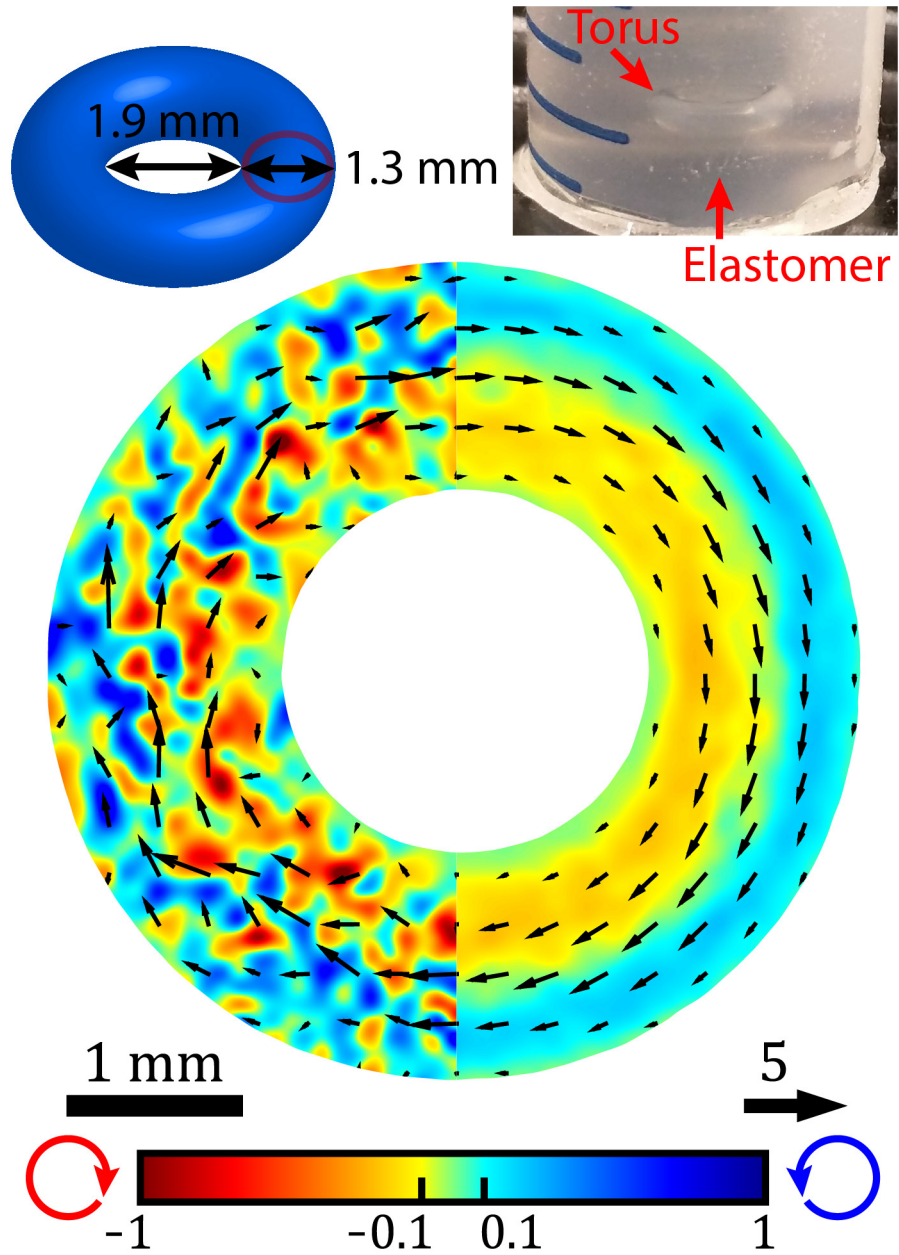


Fig. S4 Coherent flows confined in elastomers. Self-organized flows of an active fluid are confined within a torus inscribed in an elastomer. The active fluid develops a coherent clockwise circulation.

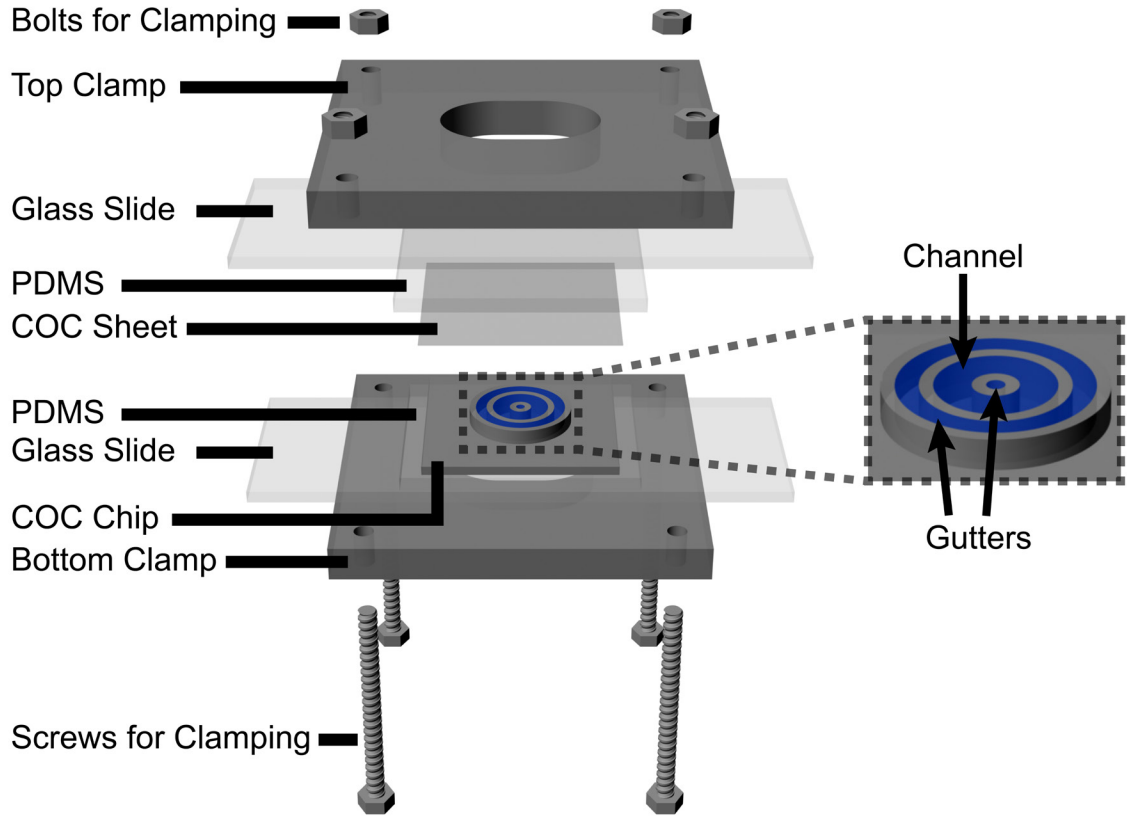


Fig. S5 Clamping a microfluidic device for confining active microtubules. To prevent evaporation the device is sealed with a clamp; the sample remains hydrated for days.

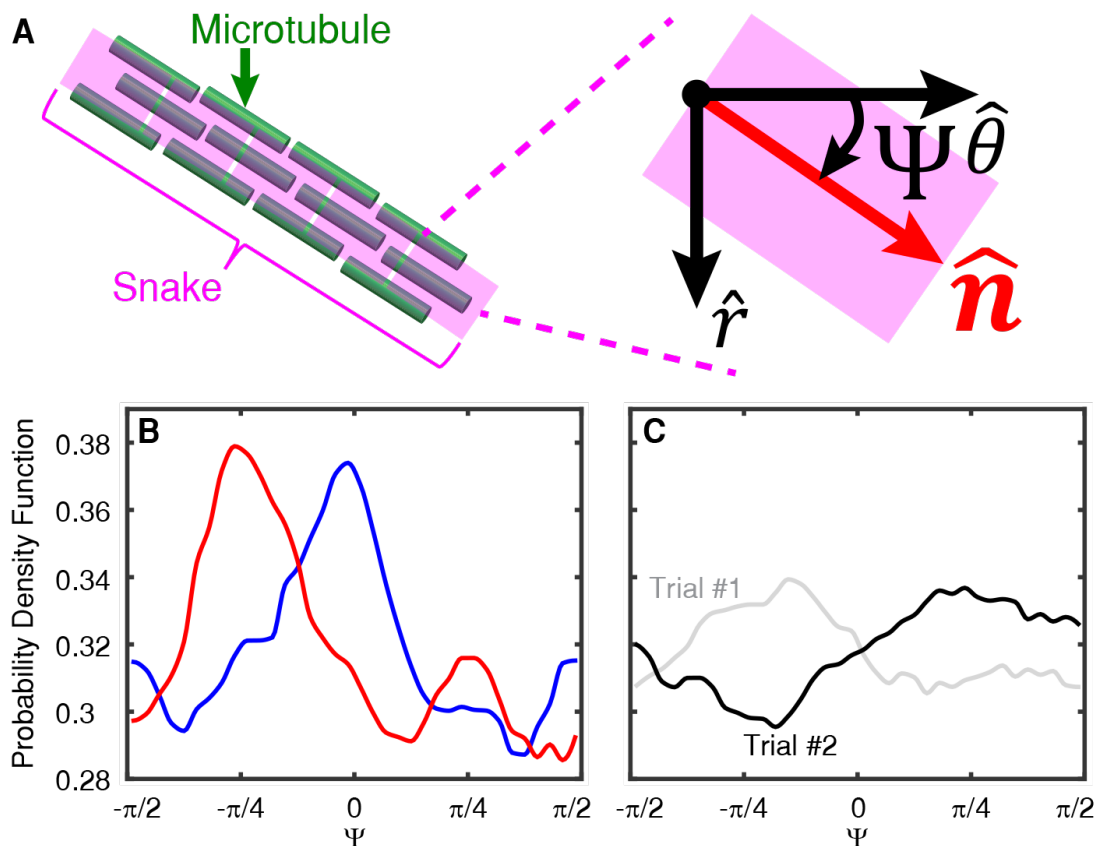


Fig. S6 Orientational distribution of bundle segments in an isotropic suspension. (A) Microtubule network structures is described by snakes, composed of unit length segments. Segment orientations in the x-y plane are characterized by director, \hat{n} , angled to $\hat{\theta}$ -axis by Ψ . (B) The distribution of bundle segments from the original (blue) and $(-\pi/4)$ -rotated (red) 3D images demonstrates that the network reconstruction algorithm has a slight bias for detecting segments that are preferentially aligned along 0 and $\pi/2$ degrees. In the red curve both the image and the reference frame is rotated by 45 degrees. The peak shift implies an artifact along image x-y axes. (C) The distributions of orientations stacked from one original and eleven structure that are rotated by 30° images. Gray and black curves represent two independent measurements, and the probability distribution function is flat to within a few percent. The isotropic suspension is confined in a cuboid whose length, width and height are 18,000, 14,000 and 90 μm , respectively.